Evolution of NiO Island Size Distributions during the Oxidation of a Ni−5Cr Alloy: Experiment and Modeling

Rohit Ramanathan,*,† Gopalakrishnan Ramalingam,‡ John H. Perepezko,*,§ Petra Reinke,*,‡ and Peter W. Voorhees†

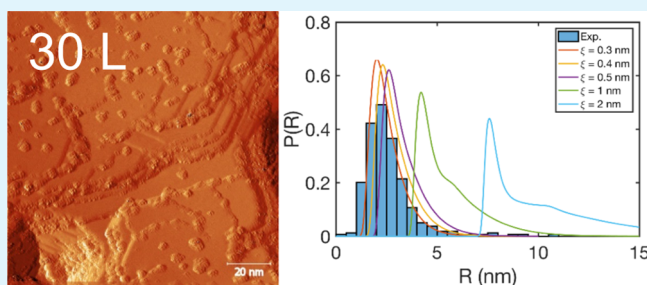†Department of Materials Science and Engineering, Northwestern University, Evanston, Illinois 60208, United States
‡Department of Materials Science and Engineering, University of Virginia, Charlottesville, Virginia 22904, United States
§Department of Materials Science and Engineering, University of Wisconsin, Madison, Wisconsin 53706, United States

Ⓢ Supporting Information

ABSTRACT: The classic models of metal oxidation developed by Wagner and Cabrera and Mott presuppose the existence of a planar oxide film and develop expressions for the rate at which the film thickens. Missing from those models is a description of how that initially planar film forms. Using scanning tunneling microscopy, we study the growth of NiO islands on the (100) surface of a Ni−5Cr alloy during the oxidation regime where the initial planar film is formed as oxide islands. The island height and area distributions as a function of the oxygen exposure in Langmuir (1 L = 10^{-6} Torr s) are measured. Lateral island growth and thickening occur as

seemingly separate processes, and after a critical thickness of ≈0.4 nm is achieved, growth is purely in the lateral direction. We develop a surface diffusion model for the evolution of the island size distribution that accounts for the lateral growth and coalescence of the NiO islands. Our results indicate that the oxygen surface diffusion screening length $\xi = \sqrt{D\tau}$ controls the island evolution. The screening length is found to be 0.3−0.4 nm, which suggests that the processes leading to island growth are highly localized to the island edge.

KEYWORDS: oxidation, alloys, STM, kinetics, surface diffusion, island growth

1. INTRODUCTION

The extended use of technical metals and alloys in their working environment often depends on the formation of a protective oxide film on the metal surface. The thin oxide film that forms on the surface acts as a barrier between the metal and the environment, shielding the metal from unwanted oxidation or corrosion that degrades its integrity.[1] Alloys that are used in high-temperature applications or aqueous environments have compositions that promote the formation of dense oxides such as Al_2O_3 or Cr_2O_3 that are especially effective as barrier layers.[2] To design new alloys with enhanced oxidation or corrosion resistance, it is important to study the development of the initial surface nucleation and growth steps that are critical to the transformation from alloy to oxide.

Two theories are often used to describe the formation of the passive film on the metal during oxidation. In the limit of a very thin film, the Cabrera−Mott theory holds, whereas for thicker films, the Wagner oxidation theory holds. Both models propose that growth of the film is due to the motion of cation or anion vacancies in the presence of an electric field. In the Cabrera−Mott model, the field is due to electron tunneling across the film,[3] whereas in the Wagner model, the field arises due to ambipolar diffusion in the oxide.[2,4] The growth laws predicted by the two models rely on the assumption that the film is growing uniformly over the surface; that is, they presuppose the existence of a planar oxide film and describe how this film thickens. The formation of the initial thin film is not described by the Cabrera−Mott model, and thus we center our attention on this "pre-Cabrera−Mott" regime.

In the pre-Cabrera−Mott regime, nucleation, followed by growth and coalescence of discrete oxide islands, leads to the formation of a passive film that covers the entire surface. The positions and sizes of these islands will impact the morphology of the resulting film, especially with respect to the formation of grains and grain boundaries. Such defects in the oxide film can be undesirable and may act as sites where oxidation or corrosion of the underlying metal is accelerated. In particular, grain boundaries can act as short-circuit diffusion paths, enhancing oxidation rates.[5−8]

Many authors have studied the formation and growth of oxide islands on the surface of pure metals. In the earliest studies of the oxidation of Mg(100) and Ni(100) by Orr[9] and Holloway and Hudson,[10] respectively, the evolution of the oxide morphology was studied using Auger spectroscopy and

Table 1. Summary of the STM Results, Including the Conditions Used for each Oxidation Step[a]

cum. O_2 exposure (L)	P_{O_2} (Pa)	time (s)	$\langle R \rangle$ (nm)	N_{tot} (m^{-2})	Θ (%)
7	4×10^{-7}	2650	1.57 ± 0.04	$1.63 \pm 0.63 \times 10^{16}$	16.8 ± 1.1
30	2×10^{-6}	1530	2.60 ± 0.07	$9.96 \pm 1.69 \times 10^{15}$	22.6 ± 5.2
80	4×10^{-6}	1663	2.94 ± 0.18	$8.43 \pm 0.88 \times 10^{15}$	31.8 ± 9.1
130	1×10^{-5}	333	4.30 ± 0.15	$5.89 \pm 1.19 \times 10^{15}$	38.8 ± 1.3

[a]After each step, images are recorded and analyzed to yield island statistics. $\langle R \rangle$: mean oxide island radius distributions are shown in Figure 2, N_{tot}: number of islands per unit area, Θ: percent of surface area covered with oxide islands.

thus information about the fractional surface coverage could be obtained but information about the individual islands, their size, and spatial distribution was lacking. These authors conclude that oxide island growth is two dimensional. Later experiments by Yang and co-workers[11−14] studied the Cu/Cu$_2$O system and were performed using transmission electron microscopy. They measured the island number density and surface coverage as a function of time and found that Cu$_2$O island growth could be two dimensional or three dimensional, depending on the orientation of the Cu substrate.

In all of the above experiments, efforts were made to develop relatively simple models to explain the island growth behavior. A general consensus has emerged that surface diffusion of oxygen to the edge of the islands drives their growth.[10,12] The models developed are based on the framework of the Johnson–Mehl–Avrami–Kolmogorov equation and focused on how the surface coverage evolves in time. Separate equations have been derived to describe the island number density evolution during the nucleation regime,[11] which rely on fitting parameters to experimental data. None of these studies made use of experimental measurements of the island size distribution and therefore the effect of the distribution of island sizes on the development of the passive oxide film could not be ascertained. Furthermore, the mean island size, a quantity typically tracked during growth and coarsening of precipitates, was not measured in these experiments.

We seek to extend the existing models by studying the postnucleation growth of NiO islands on the (100) surface of a Ni−5Cr alloy using a combination of scanning tunneling microscopy (STM) and thermodynamic/kinetic modeling. Using STM, we are able to observe the evolution of oxide islands and surface morphology during the oxidation of NiCr alloys. STM measurements are used to determine both the island height and island area, which allows for two-dimensional and three-dimensional growth of the islands to be distinguished. By analyzing the STM images, the sizes of individual islands, the island number density, and oxide surface coverage are measured as a function of oxygen exposure. This provides a rich data set that is used to develop and test our theoretical models. We develop a model for island growth and coalescence that explicitly accounts for the size distribution of islands and use it to determine how various kinetic parameters impact the evolution of the size distribution. The model is based on a surface diffusion equation for the lateral growth of islands and is implemented as a finite-difference code to track the evolution of the island size distribution. Our model handles the evolution of the number density, mean island radius, and surface coverage simultaneously. Our experiment was unable to capture the nucleation of islands in the pre-Cabrera−Mott regime. This aspect of the oxidation process will be addressed in a future manuscript.

2. EXPERIMENTAL METHODS

The oxidation of NiCr alloys with composition of Ni and Ni−5Cr was observed with an Omicron Nanotechnology variable temperature scanning probe microscopy (VT-SPM) system under ultrahigh vacuum (UHV) conditions and a base pressure <3 × 10^{-10} mbar. Alloy deposition and oxidation steps were performed in situ in a preparation chamber, and the samples were transferred to the STM without exposure to air. Epi-polished MgO(100) crystals (CrysTec GmbH) are used as substrates for thin-film growth. A recent publication[15] described the details of substrate preparation, which consisted of a multistep annealing and etching process. This enabled us to achieve smooth alloy surfaces with terrace widths exceeding on average 20 nm. Ni (Alfa Aesar, 99.999% purity) and Cr (American Elements, 99.95% purity) are deposited by electron beam evaporation using a Mantis EV mini e-beam evaporator (QUAD-EV-C) on a substrate held at 673 K. The deposition rates of Ni and Cr are measured using a quartz crystal monitor, and the deposition time is adapted to achieve a film thickness of about 30 nm. The Ni flux is maintained between 0.30 and 0.35 nm/min, and the Cr flux (0.01−0.14 nm/min) is adjusted to obtain the required composition of the alloy. Ultrapure oxygen is introduced through a needle valve and rapidly reaches the requisite pressure setpoint. The alloys are exposed to a specific oxygen dose (in Langmuir (L)) and then studied with STM. One Langmuir is defined as the flux of particles that reach the surface at a pressure of 1.33 × 10^{-6} mbar in 1 s, and it is equivalent to one monolayer assuming a sticking coefficient of one. The exposure times and corresponding O$_2$ pressures are summarized in Table 1, and all oxidation experiments were performed at 573 K. The partial pressure had to be varied throughout the experiment so that the entire range of exposures, which spans 2 orders of magnitude, could be assessed.

The as-grown thin films are characterized in situ by STM. Imaging is performed at room temperature in constant current mode with W tips that are prepared by electrochemical etching. Empty- and filled-state images are recorded on the different films; low bias voltages (V_b < 0.2 V) and set-point currents greater than 0.5 nA resulted in good quality images of the alloy surface. For oxide islands on the Ni−5Cr alloy, the best imaging conditions correspond to 2 V and a current of 0.1 nA, when the images are dominated by tunneling events from the oxide. It should be noted that STM records apparent heights and care was taken to establish reproducible imaging conditions across all experiments. The composition of the alloy thin films is confirmed ex situ by energy dispersive spectroscopy performed in an FEI Quanta 650 scanning electron microscope, which gives a composition of Ni−5Cr with an error below ±0.25 in the Cr content, and film thickness estimates are confirmed by X-ray reflectometry; both measurements are performed after the UHV experiments are finalized.

STM images were analyzed with Gwyddion,[16] an open source software for SPM data analysis. The raw STM images are not leveled, and thus additional processing of images is needed prior to segmentation. The plane leveling operation was performed followed by linear background subtraction so that the metal surface is flat in the processed data. The background is calculated and subtracted from the images on a line by line basis. For segmentation of the oxide islands, masks are created using a combination of automatic height, slope, and curvature thresholds offered by Gwyddion. The automatic thresholding sometimes led to an overestimation of the island size, and the masks are manually adapted to provide the best visual match between
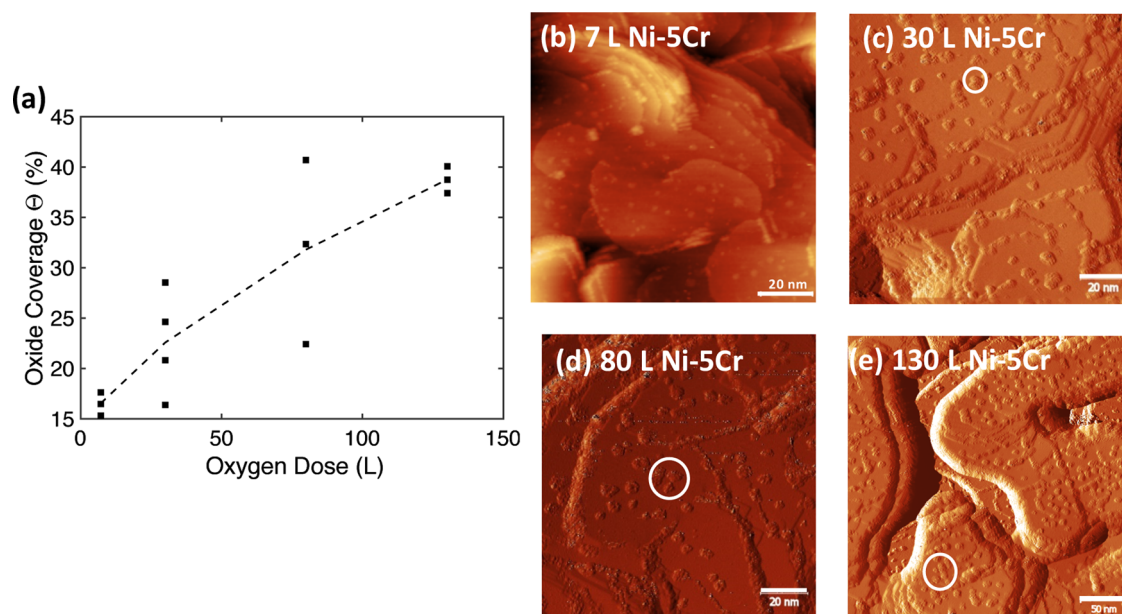
Figure 1. (a) Oxide coverage as a function of oxygen exposure given in Langmuir (L) for Ni−5Cr; the broken line serves as guidance for the eye. Several images in different areas of the sample were analyzed for each oxidation step, and representative images are shown here. (b) Ni−5Cr after 7 L, topography image with a scale bar 20 nm, (c, d) Ni−5Cr at 30 and 80 L are shown as current images (differential topography) to enhance contrast of oxide islands, scale bar 20 nm, and (e) at 130 L for Ni−5Cr, scale bar 50 nm. The images are recorded at 2 V and 0.1 nA. The areas circled in white show instances of islands touching and coalescing.
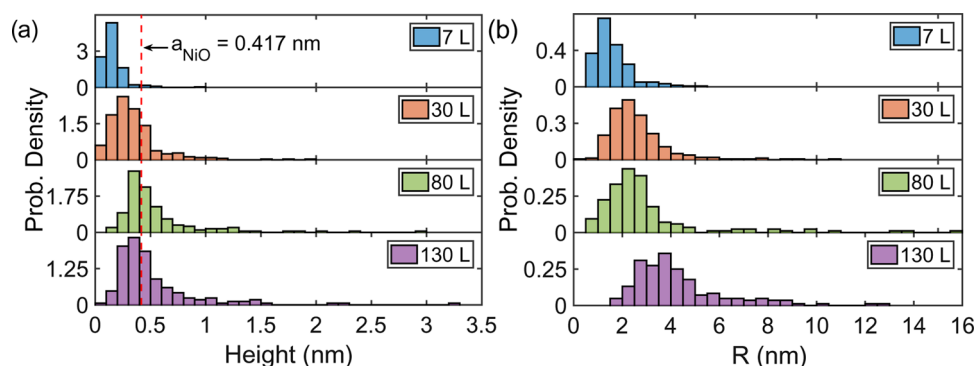

Figure 2. Histograms for the evolution of the (a) oxide island height and (b) radius distributions. The histograms are normalized to give probability density so that the total histogram area is 1. The location of the NiO lattice parameter is marked by the red dashed line. Segmentation of the STM images gives island areas, which have been converted to the radii of equivalent area circles.

masks and islands. In general, size and area data for island radii smaller than 1 nm cannot be captured reliably, which is reflected in the choice of bin size in the distributions.

3. EXPERIMENTAL RESULTS

Alloy thin films with the composition Ni−5Cr were oxidized in a controlled manner at 573 K substrate temperature using between 7 and 130 L of O_2. Figure 1 shows the oxide coverage as a function of oxygen exposure and includes representative images for oxidation of Ni−5Cr. At high oxide coverages, which are typical for alloys with higher Cr content, the large degree of island coalescence prohibits measurement of an accurate size distribution and illustrates the rapid growth of the initial oxide layer. STM data are available for oxide island evolution for several alloy compositions, and the complete range of oxygen exposures (7−130 L). A selection of STM images across all alloy compositions and oxidation steps, as well as for the Ni(100) surface is included in the Supporting Information Figure S1. A quantitative comparison with theory is best achieved for the Ni−5Cr alloy where the widest range of reliable oxide island distribution measurements could be obtained. A masking algorithm is used to extract the projected island area, which can be transformed to a radius

distribution based on the near circular shape of most islands and yields the island density as well as surface coverage. These size distributions are summarized in Figure 2.

A pure Ni(100) surface did not show any oxide islands under equivalent conditions, and the sticking coefficient for O_2 is indeed exceptionally low.[17] This has been attributed to the stability of the $c(2 \times 2)$ reconstruction with chemisorbed oxygen, which delays nucleation of oxide islands. The $c(2 \times 2)$ oxygen reconstruction forces a straightening of the step edges to align them with reconstruction.[18] The step edge kinks, which are preferred nucleation sites, disappear, and hence oxide nucleation is suppressed. This mechanism seems to fail in the NiCr alloys, and oxide islands form rapidly under otherwise identical conditions. The step edge evolution is shown in detail in the Supporting Information Figure S1.

In our work, we see this effect clearly on a pristine Ni(100) surface that is initially rich in step edges with numerous kinks, following roughly the topography defined by the underlying MgO substrate.[15] After exposure to only a few L of O_2, the kinks disappear and the step edges straighten in excellent agreement with previous findings,[18] thus removing preferential oxide nucleation sites from the surface. In NiCr alloys with low Cr concentration, it is still possible to identify a few

straight step edge segments, which indicates that small segments of the surface are reconstructed domains. The majority of step edges remain kinked and relatively rough, as can be seen in Figure 1. This removes the constraints on NiO nucleation and promotes oxide island formation.

The literature on NiCr alloy oxidation and oxide scale growth agrees that NiO will form more rapidly despite the fact that Cr_2O_3 is thermodynamically favored.[19−21] However, Cr_2O_3 growth is severely limited by the low Cr concentration in the alloy and slow Cr diffusion in the alloy at 573 K. The band gaps of the oxide islands measured with scanning tunneling spectroscopy agree with NiO values, but STM is not an element specific method and we cannot assign a specific chemical composition to each oxide island. On the basis of the STM images, the NiO appears to be highly defective. It should be noted that from the modeling perspective, very similar results, including the screening length, are obtained for NiO and Cr_2O_3. Only the input parameters, namely, the oxidation driving force and interfacial energies, are different for these cases.

The island number density as a function of the oxidation exposure in Langmuir is given in Table 1, and the number of islands continuously decreases in the course of the oxidation process. Possible mechanisms for the decrease in island density include Ostwald ripening and island coalescence. Ostwald ripening is a competitive growth process whereby small islands shrink while large islands grow and coalescence of islands consists of two islands merging to become one when they touch. On the basis of the STM images in Figure 1, we assume that coalescence is the dominant mechanism behind the decrease in the island density. The images show several instances where two islands are touching and merging, which are circled in white. In Figure 2b, we plot the island radii distributions as a function of the oxygen exposure. The classical Lifshitz−Slyozov−Wagner theory of Ostwald ripening predicts size distributions that have tails at small radii as opposed to large radii,[22,23] lending additional evidence that ripening is not the mechanism behind the reduction in the island density. Furthermore, Vincent[24] has shown that coalescence of islands leads to island size distributions whose shape is similar to that shown in Figure 2b.

Figure 2 shows the evolution of the measured island height and radius distributions as a function of oxygen exposure. The islands initially increase in height until they reach about the height of a NiO unit cell (a = 0.417 nm), which is the position of the maximum in the distribution for exposures exceeding 30 L. The island height did not change in STM images taken with different bias voltages between 1 and 4 V, which confirms that the height measurements are controlled by morphology rather than the local density of states. Lateral growth is subsequently preferred, and the island diameter starts to increase more rapidly and the surface is slowly covered with an oxide layer. At the same time, a reduction in the island density indicates the onset of coalescence, as discussed in the previous paragraph. The island size distributions are used for a direct comparison between the model and experiment.

The observation of a limiting height, which corresponds approximately to the NiO unit cell dimensions, warrants a brief discussion. If the oxide islands were crystalline, then the massive lattice mismatch between Ni and NiO (18.4%) could lead to a small critical thickness before a misfit dislocation is formed to compensate the large strain. However, the islands, grown here at a relatively low temperature, are observed to be of poor crystalline quality (highly defective), which suggests that strain is likely not a significant factor in limiting the island height. We postulate that the height is limited by the activation barriers for atom attachment to the top surface versus the sides of the island. Attaching atoms to the top of the island from the alloy surface would rely on those atoms overcoming an inverse Ehrlich−Schwoebel barrier at the island edge. In contrast, atoms attaching at the edge of the island would not need to overcome this barrier. There are likely several defect sites at the island edge to which oxygen atoms can easily attach, and thus lateral growth is favored over thickening.

The switch to lateral growth might also be attributable to wetting of the NiCr alloy surface, with NiO promoted by the strong chemical interaction between oxide and alloy bonding at the interface. Both mechanisms favor the formation of a continuous oxide layer and agree with the experimental observation of a small critical thickness.

4. ISLAND GROWTH AND COALESCENCE MODEL

4.1. Motivation and Assumptions. The STM experiments provide a rich data set for modeling purposes, including the full island size distribution, as well as measurements of the mean island size, island number density, and surface oxide coverage as a function of oxygen exposure. The mean island radius, island number density, and surface coverage can be computed from the size distribution function alone; thus, we focus our attention on modeling the evolution of this function. Myhr and Grong,[25] as well as Perez et al.,[26] have developed a finite-difference scheme for computing the evolution of size distributions due to growth of particles, and their approach is extended to describe the evolution of the island size distribution, including both growth and coalescence. Modeling the evolution of the size distribution function offers a relatively simple way to account for the kinetics of the oxidation transformation without the need to explicitly track the positions of the individual islands.

On the basis of the collected STM data, we consider the growth of islands to be two dimensional and neglect the thickening of islands. For the evolution from 30 to 80 L, the growth is almost entirely in height, whereas for the evolution from 80 to 130 L, the growth is almost entirely in lateral direction. Because the oxide surface coverage and number density evolve due to lateral growth and coalescence, we focus on modeling these processes. On the basis of this, we choose to model the islands themselves as circular disks with fixed height given by the critical height observed in the experiments.

We assume that surface diffusion of oxygen leads to growth, as suggested by several authors.[9,10,12] Because the alloy surface is an essentially unlimited source of Ni, transport of Ni is assumed to be unrestricted and thus Ni is always available to react to form more oxide at the island edge. The alloy is assumed to follow a Raoultian behavior that allows activity coefficients to be chosen to match the alloy compositions.

We note that the validity of our model is limited to surface coverages below about 40%. This is because the growth equation is only valid for circular (or nearly circular) islands. As the oxide coverage increases, the surface morphology becomes dominated by the coalescence and the shape of the islands becomes decidedly noncircular (see the Supporting Information). The growth model thus breaks down at high oxide coverages, and the model cannot describe the evolution to a surface fully covered by NiO. On the basis of the data sets for the alloys with larger chromium contents, significant deviation of the island shape form circles seems to occur when the surface coverage is about 40%. This coverage limit was not reached for the Ni−5Cr data set.

The model is based on the following equations:

1. An equation for the growth rate of islands

2. An equation for the oxygen concentration at the oxide/ alloy/gas triple junction (hereafter referred to as the interfacial concentration)

3. An equation describing island coalescence

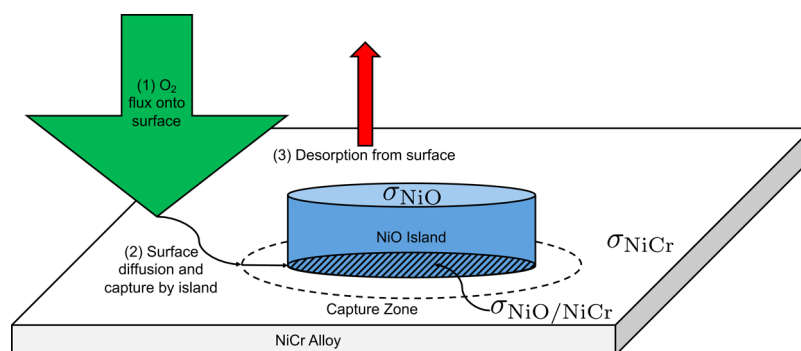4. A master evolution equation for the size distribution function that combines all of the previous equations

Figure 3. Schematic of the processes involved in the growth of an oxide island. The schematic assumes that the first process to occur is (1) flux on to the surface and then by diffusion along the surface, followed by either (2) capture by the growing the island or (3) desorption. The relative sizes of the block arrows indicate our assumption that the flux on to the surface is much greater than the desorption rate. The surface energies σ_{NiO}, $\sigma_{NiO/NiCr}$, and σ_{NiCr} are also labeled.

In the following sections, we develop these four equations. Readers interested in the full derivation of the interfacial concentration should refer to the Supporting Information.

4.2. Island Growth Rate. Figure 3 shows the surface processes involved in the growth of the island, namely, (1) flux of O_2 from the gas to the surface, (2) diffusion of oxygen along the surface, and (3) desorption of oxygen from the surface. We consider diffusion of O^{2-} on the surface and assume that dissociation of oxygen molecules happens instantaneously once the molecules hit the alloy surface. We do not consider oxygen diffusion through the bulk of the island to contribute to the lateral growth of the islands. Surface diffusion and desorption directly compete with each other: an oxygen ion either both diffuses and is captured by a growing oxide island, or it desorbs after diffusing a short distance. Note that although data for oxygen solubility in NiCr alloys is lacking, the solubility of oxygen in both pure Ni and pure Cr is small such that we do not consider bulk diffusion of dissolved oxygen in the alloy to be important for the island growth process.

The steady-state diffusion equation that describes these processes is

$$D\nabla^2 c - \frac{c}{\tau} + F = 0 \tag{1}$$

where D is the oxygen diffusion coefficient, ∇^2 is the Laplacian in polar coordinates, c is the oxygen concentration on the surface, τ is the surface residence time of oxygen on the alloy surface, and F is the gas flux on the surface. We impose the boundary conditions $c(R) = c_I$ and $c(\infty) = F\tau$, where R is the radius of the island and c_I is the interfacial oxygen concentration. The boundary condition at $r = \infty$ states that the oxygen concentration far away from the island is given by the balance between the gas flux and desorption.[27,28] Solving eq 1 and considering the mass balance at the interface,[22,29] we find the lateral growth velocity $V(R)$ is

$$V(R) = \frac{D(F\tau - c_I)}{\xi(c_{ox} - c_I)} \frac{K_1(R/\xi)}{K_0(R/\xi)} \tag{2}$$

where c_{ox} is the oxygen concentration in the oxide and $\xi = \sqrt{D\tau}$ is the diffusion screening length. K_0 and K_1 are modified Bessel functions of the second kind.

4.3. Interfacial Concentration. For the interfacial concentration c_I, we assume the reaction to form the oxide at the island edge is fast and thus the mobility of the interface is large. In the limit of infinite interfacial mobility, we recover the Gibbs−Thomson equation for the interfacial concentration that describes local equilibrium at a curved interface (see the Supporting Information for full derivation)

$$c_I(R) = c_{eq} \exp\left[\frac{V_m}{R_g T}\left(\frac{\sigma_{NiO} + \sigma_{NiO/NiCr} - \sigma_{NiCr}}{h} + \frac{\sigma_{NiO}}{R}\right)\right] \tag{3}$$

where c_{eq} is the concentration of oxygen that is in equilibrium with gas, alloy, and oxide and is related to the activity of Ni and is proportional to equilibrium oxygen pressure from the Ellingham diagram (see the Supporting Information). V_m is the molar volume of the oxide, and the term in the square brackets represents how the free energy of a circular disk island with radius R and height h is modified due to the presence of interfaces.[30,31] The σ's are the energies of the various interfaces considered and are labeled in Figure 3. All of the thermodynamics of oxide formation are packed into the expression for c_I, as shown in the Supporting Information.

The critical assumption in deriving eq 3 is that the interfacial mobility is infinite. This essentially corresponds to assuming that the activation energy for the oxidation reaction at the island edge is very small and thus the reaction can proceed as soon as oxygen diffuses to the island edge.

The value of c_I relative to $F\tau$ determines whether the island grows ($c_I < F\tau$) or shrinks ($c_I > F\tau$). c_I will decrease with increasing island radius. For the smallest islands, we must constrain $c_I < c_{ox}$ so that the growth rate does not become positive again for extremely small islands which is unphysical. We now have the equations needed to describe the growth of islands due to diffusion. Coalescence of islands on the surface is treated in the next section.

4.4. Island Coalescence. The experimental island statistics show that the island number density decreases as oxidation proceeds. This decrease is accompanied by an increase in the oxide coverage due to growth of islands. Growth of islands alone would not lead to a decrease in the island density. We consider island coalescence to be the mechanism responsible for the observed decrease in the number density of islands on the surface, as opposed to Ostwald ripening. Coalescence consists of two islands merging to become a single island, thus reducing the number of islands. Ripening of islands will only happen if some of the islands shrink due to the interfacial

concentration exceeding the far-field concentration $F\tau$. The interfacial concentration is plotted in Figure 6. On the basis of this plot, c_I does not achieve appreciable values except for very small islands ($\approx 0.1-0.2$ nm). In the postnucleation regime, the vast majority of islands are larger than this and thus island ripening will not occur. However, island coalescence is seen in the STM images and accounts for the tail of the distributions at large radii.[24]

We consider static island coalescence, meaning that the islands are not mobile on the alloy surface but coalesce when they grow and their edges touch. Instantaneous island shape relaxation is assumed so that when islands of size R_1 and R_2 and the same height coalesce, a new island of size $R_3 = (R_1^2 + R_2^2)^{1/2}$ forms.

Island coalescence is described as a population balance for the size distribution function, and thus it is useful at this point to define this function. The size distribution function $f(R, t)$ is the function with the property that $f(R, t)dR$ gives the number density of islands with radii in the range $[R, R + dR]$ at time t. An evolution equation for f can be written as

$$\frac{\partial f(R, t)}{\partial t} + \frac{\partial}{\partial R}[V(R)f(R, t)] = S(R, t) \tag{4}$$

where the second term on the left describes how f changes due to island growth and $S(R, t)$ is a term describing sources and sinks for islands.[22,23] The product $V(R)f(R, t)$ can be thought of as the island density flux in radius space, and thus eq 4 is a conservation law for f.

Equation 4 is usually considered in the case of coarsening, where $S(R, t) = 0$.[23] However, a coalescence event is a sink for the islands that merge and source for the resulting large island. The balance between the destruction of small islands and creation of large islands by coalescence is described by the Smoluchowski coagulation equation, which gives the source and sink term as[24]

$$S(R, t) = \frac{1}{2}\int_0^R \mathcal{K}(R', \sqrt{R^2 - R'^2})f(R', t)$$
$$f(\sqrt{R^2 - R'^2}, t)\,dR' - f(R, t)\int_0^\infty \mathcal{K}(R, R')$$
$$f(R', t)\,dR' \tag{5}$$

The first term of eq 5 corresponds to the formation of islands of radius R, whereas the second term corresponds to the destruction of such islands. The factor of 1/2 prevents double counting of coalescences. Equation 5 is a population balance equation for the size distribution function. Whenever an island of size R is created through coalescence, the two islands that coalesced to form it are removed from the distribution and coalescences involving an island of size R result in the removal of that island from the distribution. The function $\mathcal{K}(R, R')$ is known as the coalescence kernel and describes the rate at which coalescences occur. Assuming a random distribution of islands on the surface, it is given as

$$\mathcal{K}(R, R') = 2\pi(R + R')(V(R) + V(R')) \tag{6}$$

which can be thought of as the rate of change in the collision cross section for islands with sizes R and R'.[24,32]

4.5. Computational Details. We use a finite-difference code to solve eq 4, with the source term given by eq 5. A one-dimensional grid is created with grid spacing ΔR such that each grid point $R_i = i\Delta R$. The total number density of islands with radius R_i is given as N_i, where $N_i = f(R_i, t)\Delta R$. The growth term of eq 4 is computed using the Euler-like approach described by Perez et al.,[26] and the coalescence integrals in eq 5 are computed using Riemann sums. At each time step of the simulation, both the growth and coalescence contributions to the size distribution evolution are computed. It is important to note that these integrals have an upper limit of integration at $R = \infty$ that cannot be computed. To work around this, we choose the max radius in the grid to be at least two times as large as the largest island radius in the initial condition $R_{max,IC}$ so that the island produced by coalescence of an island with size $R_{max,IC}$ with another island of the same size is included on the computational grid and the population balance is maintained. A discussion of the convergence of the solutions can be found in the Supporting Information.

At each time step in the simulation, we compute the number density of islands N_{tot}, mean island radius $\langle R \rangle$, and surface coverage Θ as follows

$$N_{tot} = \sum_i N_i \tag{7}$$

$$\langle R \rangle = \frac{1}{N_{tot}}\sum_i R_i N_i \tag{8}$$

$$\Theta = \pi \sum_i R_i^2 N_i \tag{9}$$

After every 50 s of real time that is simulated, the size distribution itself is saved.

Because the model, as formulated, only describes lateral growth of islands and we are seeking a direct comparison between the model and experiment, we are only able to perform simulations of the experimental steps where significant lateral growth of islands is observed. To this end, we simulate the evolution of the size distribution from the 7 to the 30 L step, and the evolution of the size distribution from the 80 to the 130 L step. These simulations are hereafter referred to as the 30 and 130 L evolutions. For the initial conditions of the 30 and 130 L evolutions, we fit log-normal distributions to the measured island radii distributions for the 7 and 80 L steps, respectively. These distributions are then scaled so that the total number density of islands matches the measured value for that oxidation step. The evolution of the size distribution to 7 L cannot be simulated using this model because this regime of the experiment involves nucleation of islands, which is not the focus of the study. Furthermore, the oxidation regime from 30 to 80 L is not simulated because the relative lack of lateral island growth during this regime makes application of the model invalid.

4.6. Parameters. To apply the model, several parameters are specified. c_{ox} is estimated from the NiO crystal structure, assuming that the film is one unit cell thick. F is computed from the oxygen pressure using the expression from the kinetic theory of gases

$$F = \frac{P_{O_2}}{\sqrt{2\pi m k_B T}} \tag{10}$$

where P_{O_2} is the oxygen pressure, m is the mass of an oxygen molecule, and k_B and T have their usual meanings. For the Gibbs−Thomson equation (eq 3), values for the σ_s are chosen from the literature.[33−35] The remaining parameters D and τ, however, are not known. To circumvent this issue, we attempt
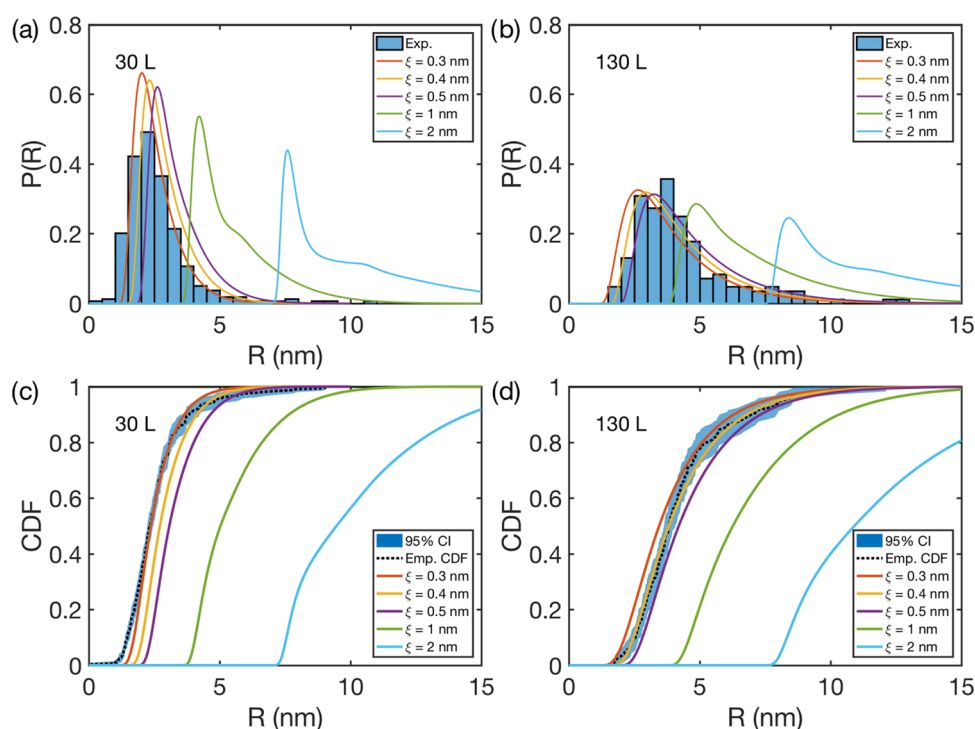
Figure 4. Comparisons of the computed and measured size distributions for the 30 and 130 L oxidation steps. (a) and (b) show the probability distribution functions for the 30 and 130 L steps, respectively whereas (c) and (d) show the cumulative distribution functions (CDF). Computed size distributions are given for screening length values of ξ = 0.3, 0.4, 0.5, 1, and 2 nm. The empirical CDF is shown along with a 95% confidence interval to show that the screening lengths of 0.3 and 0.5 nm effectively bound the STM data. Large screening length values give significant deviations from the STM data.

to the find the screening length ξ that best models the data. For each value of ξ chosen, we vary D and τ such that $\sqrt{D\tau} = \xi$. We test the following ξ values: 0.3, 0.4, 0.5, 1, and 2 nm. Values of all parameters used in the computations are given in the Supporting Information.

5. COMPUTATIONAL RESULTS AND DISCUSSION

Figure 4 compares the size distributions obtained from the computations and those obtained from the STM measurements. The distributions labeled 30 and 130 L evolved from the initial conditions are 7 and 80 L, respectively, using parameters that match the corresponding exposure from the experiment. From the plots we can see that screening length values of ξ = 0.3 and 0.5 nm bound the 95% confidence interval of the empirical cumulative distribution function (CDF). For a particular value of ξ, all combinations of D and τ led to identical size distributions, indicating that the island growth kinetics are dictated by the value of the screening length. Values of ξ smaller than 0.3 nm were not considered because these would be smaller than the smallest oxygen hopping distance on the alloy surface. Screening length values smaller than the shortest hopping distance would indicate that oxygen would desorb before a single hop could occur and growth of the islands due to surface diffusion would not be possible. Values of screening length that are larger than 0.5 nm lead to vast discrepancies between the computed and measured size distributions.

Coalescence is key to achieving a size distribution whose shape matches that found in the experiment and also captures the changes in the island number density as oxidation proceeds. Although we included coalescence primarily to account for changes in the island number density, coalescence also leads to

the observed increase in the width of the size distribution. This is because eq 5 moves islands from small radii to radii, leading to the pronounced tail in the size distribution function. Excluding coalescence from the evolution equations not only leads to no changes in the island number densities but also no changes in the shape of the size distribution function, which merely translates toward larger sizes. Thus, the overall evolution of the size distribution is due to translation caused by the growth term and broadening due to the coalescence integrals.

Table 2 shows the computed island statistics. The errors in comparison with the experiment are all less than 20% for ξ = 0.3–0.5 nm. The screening length ξ = 0.4 nm gives particularly good agreement with the STM data, with the errors all less than 10%. However, for the 30 L oxidation step, ξ = 0.3 nm seems to be more reasonable because the computed and measured distributions show better agreement at small radii, as shown in Figure 4.

The evolution of the mean radius, number density, and oxide coverage is plotted in Figure 5. From this plot, it appears that for small screening lengths (low growth rates), all three of these parameters evolve linearly in time. However, in reality, only the mean island radius increases linearly in time, whereas the number density and surface coverage evolution are nonlinear. Increasing the screening length leads to more pronounced deviations from linearity for the evolution of the number density and surface coverage. The nonlinear evolution of the number density and oxide coverage is likely primarily due to the coalescence terms in the evolution equation, where higher growth rates that accompany larger screening lengths lead to an increased rate of coalescence, which is a nonlinear process.

Table 2. Computed Island Statistics for the Size Distribution Evolutions from 7 to 30 L and 80 to 130 L[a]

ξ (nm)	$\langle R \rangle$ (nm)	N_{tot} (m^{-2})	Θ (%)
(a) 30 L Evolution			
0.3	2.55	1.12×10^{16}	25.24
0.4	2.93	9.70×10^{15}	28.60
0.5	3.33	8.43×10^{15}	31.77
1.0	5.51	4.31×10^{15}	44.34
2.0	10.29	1.52×10^{15}	54.21
exp.	2.60 ± 0.07	$9.96 \pm 1.69 \times 10^{15}$	22.6 ± 5.2
(b) 130 L Evolution			
ξ (nm)	$\langle R \rangle$ (nm)	N_{tot} (m^{-2})	Θ (%)
0.3	3.92	5.82×10^{15}	34.29
0.4	4.31	5.18×10^{15}	36.16
0.5	4.72	4.62×10^{15}	37.98
1.0	6.97	2.69×10^{15}	45.93
2.0	12.02	1.11×10^{15}	55.30
exp.	4.30 ± 0.15	$5.89 \pm 1.19 \times 10^{15}$	38.85 ± 1.3

[a]The values are shown as a function of the screening length, ξ, and the STM data is given for comparison.
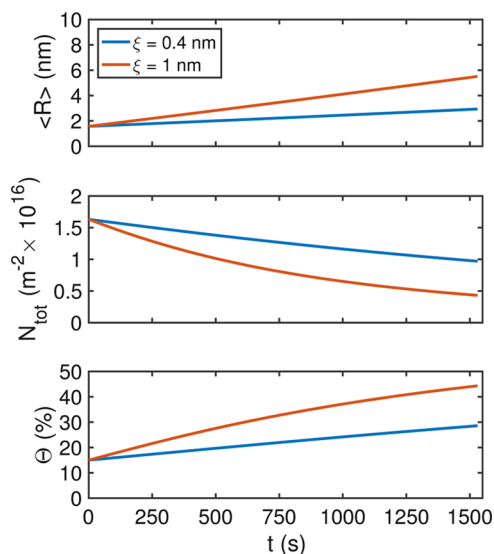

Figure 5. Evolutions of (a) the mean radius, (b) island number density, and (c) oxide coverage for the evolution from 7 to 30 L for ξ = 0.4 and 1 nm.

Control of oxide growth by the screening length alone is tied to fact that c_I is negligible for all islands with radii greater than about 0.2 nm, as shown in Figure 6. In the postnucleation regime (i.e., after the 7 L oxidation step), the vast majority of islands are larger than this. Thus, eq 2 reduces to

$$V(R) = \frac{\xi F}{c_{ox}} \frac{K_1(R/\xi)}{K_0(R/\xi)}$$

(11)

and the screening length and gas flux determine the growth rate. In fact, on the basis of ξ = 0.4 nm, the radial dependence is very weak and the growth rate is essentially constant for islands of all sizes. A constant growth rate also accounts for the linear variation of the mean island radius with time, as depicted in Figure 5.

The direct proportionality between the gas flux and the growth rate predicted by eq 11 is also supported by the STM data. For 7 to 30 L, the observed mean growth rate was $6.73 \times$
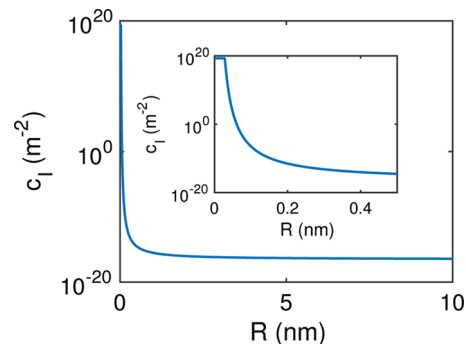

Figure 6. Plot of the interfacial oxygen concentration as a function of the island radius. The inset plot shows the behavior for the smallest islands.

10^{-4} nm/s, whereas for the evolution from 80 to 130 L, the observed mean growth rate was 4.09×10^{-3} nm/s. The 5-fold pressure increase between the two exposures would imply a 5-fold increase in the growth rate, on the basis of the reduced growth law (eq 11). The observed increase is by a factor of 6.01, which considering experimental uncertainty, is in reasonable agreement with the prediction from the model. The discrepancy again can be accounted for by the fact that the islands thicken during the exposure from 7 to 30 L.

All of the analysis presented assumes that nucleation has ceased after the 7 L oxidation step because we are neglecting nucleation contributions to the evolution of the size distribution. Having established that the growth rate of the islands is independent of size, we can make a rough estimate of the nucleation rate, J_s, from the relationship

$$N_{tot} = 0.097 \left(\frac{J_s}{V} \right)^{2/3}$$

(12)

that is derived in the Supporting Information, where V is the growth rate of the islands. Using the mean growth rate for the 7 L exposure of $V = 5.92 \times 10^{-4}$ nm/s and the resultant number density of $N_{tot} = 1.63 \times 10^{16}$ m^{-2}, we find that $J_s = 4.1 \times 10^{13}$ m^2/s. Nucleation at the steady-state rate would only need to proceed for 400 s to achieve the measured island density. Considering that the 7 L exposure occurred over 2650 s, it is quite reasonable to conclude that nucleation has ceased by the time we start taking data and our neglecting nucleation when describing the size distribution evolutions after 7 L is justified. This view is also supported by the fact that after 7 L, the island number density is continuously decreasing.

The screening length determines how quickly the oxygen concentration gradient on the alloy surface becomes zero as you move outward from the edge of the island and can be used to define a zone of capture around each island. Only oxygen atoms within the capture zone depicted in Figure 3 will contribute to growth of an island. The radius of the capture zone is a function of ξ, and a small screening length leads to slow growth because very few oxygen atoms participate in the growth process. Figure 7 plots the surface oxygen concentration relative to the far-field oxygen concentration ($F\tau$) around an island with a radius of 0.5 nm, assuming ξ = 0.4 nm. The plot clearly shows that the nonzero concentration gradient around the island extends about 3−4 screening lengths from the oxide edge, and thus we conclude that only oxygen atoms that are within 1.5−2 nm from the edge of the island can effectively contribute to growth of the oxide.
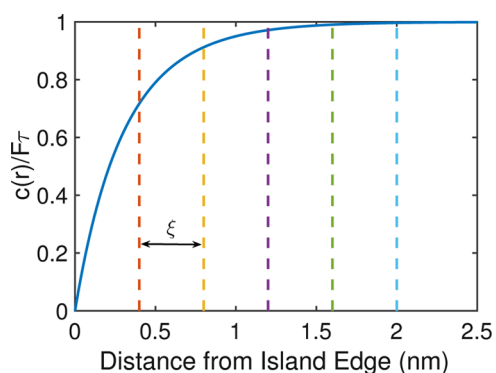
Figure 7. Plot of the oxygen concentration profile around an island. The radius of the island is 0.5 nm, and ξ = 0.4 nm. The dashed lines are placed in intervals of ξ from the edge of the island. The concentration is normalized relative to $F\tau$, the far-field oxygen concentration.

We suggest the following explanation for the slight discrepancy in the screening length for the 30 and 130 L oxidation steps, which, in principle, should be the same because the diffusivity D and desorption time τ that comprise the screening length are functions of temperature only and we are considering steady-state when such parameters should no longer be changing with oxygen coverage. During the 30 L oxidation step, the islands thicken as well as grow laterally. This means that not all of the oxygen within the screening length of the oxide edge contributes to lateral growth, as assumed in the model. Because some of the oxygen is used to thicken the island, the screening length determined from analyzing lateral growth appears smaller. The discrepancy is small although because the change in the island height is at most 0.2 nm and thus close to the detection limit of the experiment. This indicates that the oxygen uptake at the island perimeter for these small islands might occur from the alloy surface rather than from oxygen landing on the oxide island surface, but a closer examination of oxide height evolution is necessary to determine how the switch from height growth to lateral growth occurs.

A plausible explanation for the small screening length is tied to the locality of the reaction at the edge of the island. Kopatzki and Behm have used STM to confirm that the growth of an island proceeds entirely at the interface between Ni with adsorbed oxygen and the island, as proposed by our model.[36] Because this reaction is very localized, only oxygen that is close to the island can participate in a reaction to form more oxide. The screening length we find for the growth process suggests that only oxygen that is within about 3 lattice constants of the island edge can move to the island edge and react to form more oxide. In contrast to Holloway and Hudson[10] who suggested that the reaction rate at the island edge could limit growth, we postulate a fast reaction rate at the island edge and that the rate limiting step is transport of oxygen to the island edge (interface reaction-limited kinetics vs transport-limited kinetics).

In support of transport-limited growth kinetics, we attempted to model the growth using finite interfacial mobilities for determining the interfacial oxygen concentration. (see the Supporting Information). A finite interfacial mobility implies that there is a significant activation energy barrier for the oxidation reaction and thus the rate of the reaction is slow and determines the growth rate. For completely interface reaction-limited growth (small interfacial mobility), the interfacial

concentration is very close to the far-field concentration $F\tau$ and thus the growth rate is essentially 0 unless the diffusivity of oxygen is large. Because observations of oxygen diffusion on pure Ni surfaces suggest that the diffusivity is extremely small,[36,37] growth limited by interfacial reactions alone seems unlikely. In fact, a recent density functional theory study suggests that oxygen diffusivity on Ni surfaces in the presence of Cr will be even smaller than on the pure Ni surface,[38] lending additional support that reaction-limited growth kinetics are unlikely. The small growth rate of the islands is due to the fact that only very few oxygen ions can move to the island edge to react and diffusion to the island edge is likely sluggish.

Fundamentally, the screening length is tied to the diffusion coefficient and surface residence time. The diffusion coefficient can be written as

$$ D = \frac{1}{4}a^2 \nu \, \exp\left(-\frac{E_{\text{diff}}}{k_{\text{B}}T}\right) \tag{13} $$

and the surface residence time as

$$ \tau = \frac{1}{\nu} \, \exp\left(\frac{E_{\text{des}}}{k_{\text{B}}T}\right) \tag{14} $$

On the basis of the definition of the screening length, we have

$$ \xi = \sqrt{D\tau} = \frac{1}{2}a \, \exp\left(\frac{E_{\text{des}} - E_{\text{diff}}}{2k_{\text{B}}T}\right) \tag{15} $$

In these equations, a is the lattice constant of the alloy, ν is the vibration frequency of oxygen on the alloy surface, E_{diff} is the activation energy for diffusion, and E_{des} is the activation energy for desorption. The quantity $E_{\text{des}} - E_{\text{diff}}$ must be greater than 0 for surface diffusion of oxygen to occur. Assuming the lattice constant of the alloy surface is the same as that of pure Ni (0.352 nm), we find that a screening length of ≈0.4 nm is obtained if the difference in the desorption and diffusion activation energies is less than about 0.1 eV. This result is independent of the actual values of the desorption time and diffusion coefficient themselves, and thus we cannot conclude anything about the relative magnitudes of these parameters from our analysis. This energy difference could be larger if the base frequencies for desorption diffusion are allowed to differ, but those data are not available at present. In principle, the surface diffusion coefficient and adsorption kinetics could be assessed through molecular dynamics or density functional theory calculations. Clearly, there exists a significant knowledge gap in understanding of the oxygen interaction with the alloy surface, including the impact of Cr on the inhibition of the $c(2 \times 2)$ oxygen adatom reconstruction, which appears to favor rapid NiO formation, and the reactivity of the oxide island perimeter.

To put things in perspective, we compare our result to measurements of the oxygen surface diffusion coefficient on clean Ni(100) surfaces. Binnig et al.,[37] as well as Kopatzki and Behm,[36] have used STM to characterize the dynamics of oxygen adatom movement on Ni(100) and have measured diffusion coefficients as low as 10^{-24} m^2/s at room temperature and as low as 10^{-16} m^2/s at 573 K.[36,37] These extremely small diffusion coefficients could lead to the small screening length we find, depending on the exact value for the desorption time τ. On the basis of the discussion of the diffusion coefficient and desorption time in the previous paragraph, the implication of a

small diffusion coefficient is a long desorption time, although this needs to be verified by additional measurements.

6. SUMMARY

We have used a combination of STM and thermodynamic/kinetic modeling to study the growth of NiO islands on a Ni–5Cr alloy. Using the STM data, island statistics were obtained, including the island number density, surface coverage, and size distribution as a function of oxygen exposure. STM data reveals that changes in the island height and radius are a separate, rather than concurrent, process. Islands grow in height until they reach a critical thickness, after which the lateral growth dominates. A model for the evolution of the oxide island size distributions was developed on the basis of the assumption that surface diffusion of oxygen to the oxide edge is responsible for growth. The model shows that the evolution of the surface oxide morphology is controlled by the diffusion screening length, which we find to be approximately 0.4 nm. Using this value of the screening length, excellent agreement between simulated and measured size distributions and island statistics is achieved. Coalescence is needed to account for changes in the island number density as oxidation proceeds. Our results indicate that the island growth rate is essentially a constant independent of the island size and is directly proportional to the gas pressure. The combination of experimental and modeling results confirms that oxide growth in the pre-Cabrera–Mott regime is rather complex and cannot be adequately described by any model that currently exists in the literature. Future studies will focus on the earliest stages of island growth so that the nucleation behavior of the oxide can be better understood.

ASSOCIATED CONTENT

Ⓢ Supporting Information

The Supporting Information is available free of charge on the ACS Publications website at DOI: 10.1021/acsami.7b18539.

(1) STM images of oxide growth on other NiCr alloys, (2) derivation of the interfacial oxygen concentration expression, (3) discussion on our choice of c_{eq}, (4) derivation of the expression used to describe nucleation, (5) a discussion of convergence issues in the finite-difference code, and (6) a table listing values of materials parameters used in the simulations (PDF)

AUTHOR INFORMATION

Corresponding Authors
*E-mail: rohitramanathan2020@u.northwestern.edu (R.R.).
*E-mail: perepezk@engr.wisc.edu (J.H.P.).
*E-mail: pr6e@virginia.edu (P.R.).

ORCID Ⓞ
Rohit Ramanathan: 0000-0002-6961-3521
Petra Reinke: 0000-0002-4544-5906

Notes
The authors declare no competing financial interest.

REFERENCES

(1) Macdonald, D. D. Passivity-The Key to Our Metals-Based Civilization. *Pure Appl. Chem.* **1999**, *71*, 951−976.

(2) Atkinson, A. Transport Processes During the Growth of Oxide Films at Elevated Temperature. *Rev. Mod. Phys.* **1985**, *57*, 437−470.

(3) Cabrera, N.; Mott, N. F. Theory of the Oxidation of Metals. *Rep. Prog. Phys.* **1949**, *12*, 163−184.

(4) Lankhorst, M. H.; Bouwmeester, H. J.; Verweij, H. Thermodynamics and Transport of Ionic and Electronic Defects in Crystalline Oxides. *J. Am. Ceram. Soc.* **1997**, *80*, 2175−2198.

(5) Harris, A. W.; Atkinson, A. Oxygen Transport in Growing Nickel Oxide Scales at 600-800 °C. *Oxid. Met.* **1990**, *34*, 229−258.

(6) Mrowec, S.; Grzesik, Z.; Rajchel, B. Oxidation of Nickel and Ni-Cr and Ni-Na Alloys at High Temperatures. *High Temp. Mater. Processes* **2004**, *23*, 59−72.

(7) Peraldi, R.; Monceau, D.; Pieraggi, B. Correlations Between Growth Kinetics and Microstructure for Scales Bormed by High-Temperature Oxidation of Pure Nickel. II. Growth Kinetics. *Oxid. Met.* **2002**, *58*, 275−295.

(8) Lawless, K. R. The Oxidation of Metals. *Rep. Prog. Phys.* **1974**, *37*, 231−316.

(9) Orr, W. Oxide Nucleation and Growth. Ph.D. Thesis, Cornell University: Ithaca, NY, 1962.

(10) Holloway, P. H.; Hudson, J. B. Kinetics of the Reaction of Oxygen with Clean Nickel Single Crystal Surfaces I - Ni(100) Surface. *Surf. Sci.* **1974**, *43*, 123−140.

(11) Yang, J.; Yeadon, M.; Kolasa, B.; Gibson, J. The Homogeneous Nucleation Mechanism of Cu2O on Cu(001). *Scr. Mater.* **1998**, *38*, 1237−1242.

(12) Yang, J. C.; Evan, D.; Tropia, L. From Nucleation to Coalescence of Cu2O Islands During In-Situ Oxidation of Cu(001). *Appl. Phys. Lett.* **2002**, *81*, 241−243.

(13) Zhou, G.; Yang, J. C. Initial Oxidation Kinetics of Copper (110) Film Investigated by In Situ UHV-TEM. *Surf. Sci.* **2003**, *531*, 359−367.

(14) Zhou, G.; Yang, J. C. Initial Oxidation Kinetics of Cu(100), (110), and (111) Thin Films Investigated by In-Situ Ultra-High-Vacuum Transmission Electron Microscopy. *J. Mater. Res.* **2005**, *20*, 1684−1694.

(15) Ramalingam, G.; Reinke, P. Growth of Ni and Ni-Cr Alloy Thin Films on MgO(001): Effect of Alloy Composition on Surface Morphology. *J. Appl. Phys.* **2016**, *120*, No. 225302.

(16) Nečas, D.; Klapetek, P. Gwyddion: An Open-Source Software for SPM Data Analysis. *Open Phys.* **2012**, *10*, 181−188.

(17) Stuckless, J. T.; Wartnaby, C. E.; Al-Sarraf, N.; Dixon-Warren, S. J. B.; Kovar, M.; King, D. A. Oxygen Chemisorption and Oxide Film Growth on Ni{100}, {110}, and {111}: Sticking Probabilities and Microcalorimetric Adsorption Heats. *J. Chem. Phys.* **1997**, *106*, 2012−2030.

(18) Kopatzki, E.; Behm, R. J. Step Faceting: Origin of the Temperature Dependent Induction Period in Ni(100) Oxidation. *Phys. Rev. Lett.* **1995**, *74*, 1399−1402.

(19) Machet, A.; Galtayries, A.; Zanna, S.; Klein, L.; Maurice, V.; Jolivet, P.; Foucault, M.; Combrade, P.; Scott, P.; Marcus, P. XPS and STM Study of the Growth and Structure of Passive Films in High Temperature Water on a Nickel-Base Alloy. *Electrochim. Acta* **2004**, *49*, 3957−3964.

(20) Calvarin, G.; Molins, R.; Huntz, A. M. Oxidation Mechanism of Ni-20Cr Foils and Its Relation to the Oxide-Scale Microstructure. *Oxid. Met.* **2000**, *53*, 25−48.

(21) Luo, L.; Zou, L.; Schreiber, D. K.; Baer, D. R.; Bruemmer, S. M.; Zhou, G.; Wang, C. M. In-Situ Transmission Electron Microscopy Study of Surface Oxidation for Ni-10Cr and Ni-20Cr Alloys. *Scr. Mater.* **2016**, *114*, 129−132.

(22) Ratke, L.; Voorhees, P. W. *Growth and Coarsening*; Engineering Materials; Springer-Verlag: New York, 2002; pp 65−67.

(23) Hoyt, J. J. *Phase Transformations*; McMaster Innovation Press: Hamilton, ON, 2010; pp 147−154.

(24) Vincent, R. A Theoretical Analysis and Computer Simulation of the Growth of Epitaxial Films. *Proc. R. Soc. A* **1971**, *321*, 53−68.

(25) Myhr, O. R.; Grong, Ø. Modelling of Non-Isothermal Transformations in Alloys Containing a Particle Distribution. *Acta Mater.* **2000**, *48*, 1605−1615.

(26) Perez, M.; Dumont, M.; Acevedo-Reyes, D. Implementation of Classical Nucleation and Growth Theories for Precipitation. *Acta Mater.* **2008**, *56*, 2119−2132.

(27) Venables, J. A. Rate Equation Approaches to Thin Film Nucleation Kinetics. *Philos. Mag.* **1973**, *27*, 697−738.

(28) Lewis, B.; Rees, G. J. Adatom Migration, Capture and Decay Among Competing Nuclei on a Substrate. *Philos. Mag.* **1974**, *29*, 1253−1280.

(29) Voorhees, P. W.; Shahani, A. J. Unpublished Notes, 2015.

(30) Thompson, C. V. Coarsening of Particles on a Planar Substrate: Interface Energy Anisotropy and Application to Grain Growth in Thin Films. *Acta Metall.* **1988**, *36*, 2929−2934.

(31) Zinke-allmang, M.; Feldman, L. C.; Grabow, M. H. Clustering on Surfaces. *Surf. Sci. Rep.* **1992**, *16*, 377−463.

(32) Liu, S.; Bönig, L.; Metiu, H. The Effect of Island Coalescence on Island Density During Epitaxial Growth. *Surf. Sci.* **1997**, *392*, L56−L62.

(33) Pilliar, R. M.; Nutting, J. Solid-Solid Interfacial Energy Determinations in Metal-Ceramic systems. *Philos. Mag.* **1967**, *16*, 181−188.

(34) Vitos, L.; Ruban, A. V.; Skriver, H. L.; Kollár, J. The Surface Energy of Metals. *Surf. Sci.* **1998**, *411*, 186−202.

(35) Oliver, P. M.; Watson, G. W.; Parker, S. C. Molecular-Dynamics Simulations of Nickel Oxide Surfaces. *Phys. Rev. B* **1995**, *52*, 5323−5333.

(36) Kopatzki, E.; Behm, R. J. STM Imaging and Local Order of Oxygen Adlayers on Ni(100). *Surf. Sci.* **1991**, *245*, 255−262.

(37) Binnig, G.; Fuchs, H.; Stoll, E. Surface Diffusion of Oxygen Atoms Individually Observed by STM. *Surf. Sci.* **1986**, *169*, L295−L300.

(38) Alexandrov, V.; Sushko, M. L.; Schreiber, D. K.; Breummer, S. M.; Rosso, K. M. Adsorption and diffusion of atomic oxygen and sulfur at pristine and doped Ni surfaces with implications for stress corrosion cracking. *Corros. Sci.* **2016**, *113*, 26−30.